J. Electrochem. Sci. Eng. **16** (2026) 3012; https://doi.org/10.5599/jese.3012

Open Access : : ISSN 1847-9286
https://pub.iapchem.org/ojs/index.php/JESE

Original scientific paper

Environmentally benign synthesis of CuO impregnated activated carbon nanocomposite for prompt bifunctional water splitting applications

Tika Bhandari[1], Rama Kafle[1], Prakash Ban[1], Jyoti Ghorshine[1], Debendra Acharya[2,✉] and Dasu Ram Paudel[1,✉]

[1]*Department of Chemistry, Tri-Chandra Multiple Campus, Tribhuvan University, Kathmandu 44613, Nepal*

[2]*Department of Nano Convergence Engineering (BK21 Four), Jeonbuk National University, Jeonju, Jeonbuk, 54896 Republic of Korea*

Corresponding Authors: ✉*acharyadebendra88@gmail.com*; ✉*dasu.paudel@trc.tu.edu.np*

Received: September 12, 2025; Accepted: January 4, 2026; Published: January 8, 2026

Abstract

The global pursuit of sustainable energy solutions has intensified the exploration of efficient and eco-friendly methods for hydrogen production, particularly through the hydrogen evolution reaction (HER) from renewable energy sources. Our research focuses on combining bio-waste-derived activated carbon nanomaterials with green-synthesized copper oxide nanoparticles (CuO@AC) to create efficient electrode materials for enhancing HER and oxygen evolution reaction (OER). The surface features of the composite material indicate a nanoarchitectonics of rubble morphology, and multiple intense peaks provide evidence for the successful fabrication of each expected crystalline phase, reflecting the overall composition and structural integrity of the nanomaterials. Findings also make known that CuO nanoparticles combined with activated carbon exhibit high efficiency for both HER and OER activities. It required an overpotential of 137 mV at 10 mA cm^{-2} current density and a Tafel slope of 94 mV dec^{-1} to drive the HER, while an overpotential of 194 mV was required to achieve a 10 mA cm^{-2} current density and a Tafel slope of 67.9 mV dec^{-1} for the OER catalysis process. This work aims to enhance our understanding of the interactions between activated carbon and metal oxides, highlighting the potential of tailored electrocatalytic materials for sustainable energy conversion and contributing to net-zero emission targets.

Keywords

Hydrogen evolution reaction; oxygen evolution reaction; electrocatalyst; biomass-derived activated carbon; green hydrogen

Introduction

The global energy demand is increasing due to population growth and economic expansion. Natural gas, coal, and other non-renewable fossil fuels currently supply the majority of this need, which is expected to be depleted within the coming few years [1,2]. The use of fossil fuels contributes to environmental deterioration, putting human life in jeopardy by causing climate change and greenhouse gas emissions, which frequently result in costly management expenses [1,3]. Energy is beginning to constrain economic growth due to environmental pollution and energy depletion. But the majority of the energy used today comes from nonrenewable fossil fuels [4]. Thus, electrochemical energy conversion and storage device systems, along with their respective electrode reactions, are a globally significant and environmentally conscious subject [5]. Electrochemical water splitting is an effective way to address the ongoing energy crisis through sustainable energy conversion and storage. The electrochemical water-splitting process involves the oxygen evolution reaction (OER) and the hydrogen evolution reaction (HER) [6]. Hydrogen, being renewable, emits zero emissions and is environmentally benign, presenting itself as a viable alternative to fossil fuels [7,8]. It boasts a higher energy content than natural gasoline and can be sourced diversely, with the added advantages of non-toxicity and ease of storage through chemical or physicochemical means [9,10]. However, the widespread adoption of this technology in commercial applications remains constrained due to the limited availability, rising expenses, and inadequate stability of precious metals like Pt, Pd, Ru and Ir, which are essential for ensuring optimal performance in both the HER and OER [11-13]. Searching for materials that are plentiful, renewable, and sustainable is essential in this regard, which can support current needs and ensure the natural prosperity [8,14].

In the pursuit of sustainable energy sources and efficient environmental remediation strategies, the development of advanced materials plays a pivotal role. Current developments in total water splitting place considerable emphasis on transition-metal compounds, including those based on Fe, Co, Ni, Cu, V, Re, W and Mo [6,15-17]. These substances are favoured because they are inexpensive, have a high theoretical catalytic activity, are abundant in nature, and are cost-effective [8]. Several catalysts in this category have demonstrated remarkable performance for both HER and OER, and the overall potential for water splitting has even fallen below that of the benchmark Pt/C and IrO_2 electrode pairs [6]. The majority of bifunctional catalysts that have been recognized comprise transition metal oxides, carbides, phosphides, and sulphides. Moreover, the high catalytic activity is aided by thoughtful modification of their morphology and the electronic structures, which optimize their performance due to enhanced reaction kinetics, rapid charge transfer, and high conductivity [18,19]. Transition metal chalcogenides and nitrides are frequently effective catalysts for HER and may be active for OER. However, under alkaline OER conditions, they typically undergo oxidation, forming metal oxides or hydroxides on the surface or even throughout the bulk [20]. As a result, the true catalytically active species are these oxides/hydroxides rather than the initially unstable compounds. Hence, the transition metal oxides were widely developed as OER catalysts due to their affordable, abundant, and strong anticorrosion qualities in an alkaline environment [21,22]. TMOs show excellent performance for OER, but they are often less potent for HER due to poor hydrogen desorption capabilities [23]. However, significant advancements have been made in engineering TMOs to enhance their catalytic properties for alkaline HER, making them promising candidates for overall water-splitting applications. To fully harness the capabilities of TMOs, it is essential to address challenges concerning stability, conductivity, and tailored functionality [24,25]. Among them, the integration of metal oxides with environmentally friendly matrices remains underexplored. Moreover, the NPs synthesized using the green method are simple, quick, cost-effective,

efficient, and adaptable [26,27]. CuO nanoparticles are much less expensive to synthesize than other contemporary nanoparticles, which have superior electrocatalytic properties due to their peculiar crystal structure and capacity to enhance electron transfer reactions [18,28,29].

Nanostructures are highly valued for their chemical stability, electrical conductivity, and ability to host electrochemically active species via intercalation. Recently, carbon-based materials and their nanostructures have attracted significant attention due to their potential applications in energy storage, sensing, and electrocatalysis [30]. However, creating carbon nanostructures with precisely engineered architectures, surface areas, porosity, and pore-size distributions using readily available resources remains challenging. Moreover, biomass-derived activated carbons have gained popularity because they offer a large surface area, high porosity, and scalability [31]. In this context, focus has been on synthesizing carbon nanoparticles from abundant biomass resources and waste products to develop effective catalysts for energy conversion [32]. The copper oxide nanoparticles infused in activated carbon matrix (CuO@AC) can demonstrate improved HER and OER catalysis due to the synergistic contribution of the carbon-supported CuO nanocomposite. The catalytic potential of non-precious CuO can be further enhanced when supported on AC, thereby increasing the interaction of water molecules with the catalyst surface during the water-splitting reaction [33].

This study aims to bridge these gaps by investigating the production, description, and use of metal oxide nanoparticles entwined biomass-derived porous carbon matrix nanocomposites, thereby addressing the need for novel materials with enhanced electrochemical performance and potential electrochemical activity. The synthesis process is straightforward, and the use of low-cost materials makes this method not only cost-effective but also suitable for large-scale implementation. This work aims to advance the understanding of activated carbon-to-metal oxide interaction, highlighting the potential of strategic design in creating tailored electrocatalytic materials for green hydrogen production.

Experimental

Chemicals and instruments

Potassium hydroxide (KOH, 95%) and cupric nitrate [$Cu(NO_3)_2$], 98.99 % were purchased from Thermo Fischer Scientific India Pvt. Ltd, hydrochloric acid (HCl, 36 wt.%) from Lab Alley Powering Science, Urea [$CO(NH_2)_2$], 99.5 % from Oxford Lab Fine Chem Lip, and ethanol (CH_3CH_2OH, 99.20 %) from BRG Biomedicals. Laboratory mill (Grinder), Magnetic stirrer (REMI 2MLH), Centrifuge Machine (REMI R4 Laboratory centrifuge), Sieve size 150-250 µm, Weighing Balance (Phoenix instrument), Digital pH meter (SPECTRONICS INDIA, MODEL NO. S1-139), Muffle furnace (Accuma χ India, NEW DEHLI-110058), Tubular furnace (CITY INSTRUMENTS), Hot air oven (TORRE PICENARDI (CR) ITALY, Mod. PANACEA 430) were available in the laboratory.

Synthesis of activated carbon

Corncobs were collected from the local market in Tokha, Kathmandu. The corncobs, here abbreviated as CC, were finely chopped, thoroughly cleansed with deionized water. Subsequently, it was dried for 8 hours at 100 °C and then ground into a powder. After screening, irregular granules measuring 150 to 250 µm were selected. Using a nitrogen atmosphere in a tube furnace, the dried CC was calcinated for two hours at 300 °C at the rate of 5 °C min^{-1}. Subsequently, the calcined CC was mixed with a urea solution and KOH, and the mixture was aged for 6 hours. Three mass ratios were established for urea, KOH and CCs: 1:1:1. After that, the mixture was dried at 100 °C in an oven. The activation process was conducted in crucibles for 2 h at 700 °C. Subsequently, a black solid powder

was produced and thoroughly rinsed with deionized water and 1 M hydrochloric acid until the pH was neutral. Finally, the powders were dried for 12 hours at 60 °C, yielding activated carbon samples, referred to as AC [34].

Preparation of raw Allium sativum plant extract

Fresh *Allium sativum* collected from Tokha-03, Kathmandu, was rinsed with tap water and deionized water to remove external contaminants. Subsequently, approximately 5 g of Allium sativum was ground into a fine paste, and the paste was mixed with 100 mL of deionized water under continuous stirring and boiling at 70 °C for 30 minutes. Subsequently, a Whatman No. 40 filter paper was used to filter and refine the solution. The filtrate was stored in the refrigerator for subsequent use.

Synthesis of copper oxide nanoparticles via Allium sativum extract

First, 1 M cupric nitrate solution was prepared by dissolving 1 g of cupric nitrate in 80 mL of deionized water. Subsequently, 20 mL of *Allium sativum* extract was added to the mixture. The mixture was then stirred at 300 rpm at 70 °C under boiling conditions for two to three hours. The change from a blue-coloured solution to a deep green colour indicates the formation of CuO nanoparticles. The reaction mixture was then centrifuged and cleaned using deionized water and ethanol. The CuO nanoparticles were then dried overnight at 80 °C in a hot air oven. Subsequently, the heat treatment was performed in a muffle furnace at 400 °C for 3 h to remove volatile impurities and intercalated water molecules [17].

Synthesis of CuO impregnated activated carbon composite electrocatalyst

For the preparation of the copper oxide impregnated activated carbon nanocomposite, 80 mL of DI water and 20 mL of *Allium sativum* extract were mixed with 1M cupric nitrate salt. Under continuous stirring, 1 g of activated carbon was carefully weighed and gently mixed into the solution. The reaction mixture was then boiled at 70 °C for 2 hours until the solution changed from bluish to dark greenish-black. The mixture was then centrifuged and washed with deionized water and ethanol. Subsequently, the sample was dehydrated overnight at 80 °C in a hot air oven. Finally, calcination was carried out in a muffle furnace at 400 °C for 3 hours. The resulting greenish-black solid nanocomposite powder was obtained and used for further characterization [35,36].

Physicochemical characterization

An X-ray diffractometer with monochromatic Cu-Kα radiation (D_2 phase Diffractometer, Bruker, Germany) scanned at 2θ from 20 to 80°, was used at the Nepal Academy of Science and Technology (NAST) to investigate a powdered sample of CuO nanoparticles and their nanocomposite. Fourier transform infrared spectroscopy (FTIR) was used to characterize powder samples of metal nanoparticles and their nanocomposite (Llantrisant, UK. Model PEFTIR) at Amrit Science Campus (ASCOL), at 4000 to 400 cm^{-1} wavenumbers for the identification of the chemical fingerprints. The powder sample was placed in the cuvette and mounted on the device stage for the IR beam to pass through it. The transmitted light is measured, and a spectrum is generated. The morphological and structural characteristics of the sample were examined using a Zeiss Co., Germany Supra 40 VP equipment at Jeonbuk National University's Center for University-Wide Research Facilities (CURF). For FESEM imaging, a sample in powder form was utilized. Energy-dispersive spectroscopy (EDS) was used to examine the elemental composition of the catalyst.

Electrochemical characterization

At room temperature, the produced materials were electrochemically characterized using a potentiostat/galvanostat electrochemical analyzer (VersaSTAT, AMETEK Inc., USA). A graphite rod served as the counter electrode, and Ag/AgCl as the reference electrode. The electrolyte used in all electrochemical tests was 1M KOH. A solid powder (approximately 5 mg) of the electrocatalyst loaded on nickel foam (1×1 cm^2) was used for the hydrogen evolution reaction and the oxygen evolution reaction. The Ni foam serves as a substrate due to its low cost, high efficiency, excellent electrical conductivity, robust mechanical strength, and binder-free capacity to retain active materials [37]. Moreover, the structure of Ni foam has a large surface area, which facilitates electrochemical reactions [38]. Three-electrode setups were used for individual HER/OER studies, and each electrocatalyst was activated by performing 50 cycles of cyclic voltammetry within a defined voltage range. The linear sweep voltammetry (LSV) measurements were done at a scan rate of 2 mV s^{-1}, and the resulting polarization curves are plotted after *IR* correction using the equation ($E_{IR\text{-corrected}} = E_{(V\ vs.\ RHE)} - IR_s$). Here, *I* represent the current, and R_s denotes the equivalent series resistance. The alternating current used in electrochemical impedance spectroscopy (EIS) measurements was applied at an amplitude of 5 mV over a frequency range of 100 kHz to 0.001 Hz. The electrochemically active surface area (ESCA) of the electrocatalyst was calculated from cyclic voltammograms (CVs) recorded at scan rates between 20 and 100 mV s^{-1} over the potential range 1.125 to 1.225 V *vs*. RHE. A linear relationship was observed when plotting the scan rate against the difference between the anodic and cathodic currents (I_{anode} - - $I_{cathode}$), and the resulting slope indicates the electrochemical double-layer capacitance (C_{dl}). The overall ESCA of the electrocatalyst is calculated as the ratio of C_{dl} to the specific capacitance of the flat surface (C_S).

Results and discussion

The current study aims to synthesize a nanocomposite of a transition-metal oxide impregnated in a biomass-derived porous carbon matrix via a simple, green approach. The approach involves designing a low-cost, high-catalytic-activity CuO on a conductive AC framework for the development of an efficient, stable, and economical water-splitting electrode via a green synthesis method. Inspired by the key electrocatalytic properties of CuO nanoparticles and the activated carbon support, a comprehensive approach to material synthesis, structural characterization, and electrochemical assessment provides new insights into the development of advanced electrocatalysts for green hydrogen production. The rich active sites are anticipated at the interface between the porous activated carbon framework and the dispersed CuO nanostructure, resulting in a CuO@AC nanocomposite (Figure 1).

Figure 1. *Schematics showing the synthesis and potential applications of CuO@AC nanocomposite*

The composite comprises activated carbon as a conductive support and electron reservoir, along with catalytically active CuO NPs, providing synergistic interactions that enhance electron transfer, improve H2O adsorption/desorption, and activate bifunctional catalytic efficacy [28,39]. Hence, the intuition behind the composite CuO@AC nanomaterial lies in the synergistic effect, where the activated carbon creates high conductivity, a sufficient surface area, and a porous framework, thus providing an ideal environment for CuO to perform optimally and overcome its inherent electro-catalytic limitations [24,33].

Morphological characterization

The overall morphology, relative size, and dispersion of the as-synthesized CuO-NPs and CuO@AC nanocomposite were examined using FE-SEM analysis. Additionally, the chemical composition, elemental proportions, and distribution were investigated using energy-dispersive X-ray (EDX) colour-mapping images and spectra (Figures 2 and 3) [40]. The copper oxide nanoparticles appeared to have a well-defined texture, with irregular, clustered structures of various shapes and sizes (Figure 2a to 2c). The images in Figure 2a show the overall surface quality of the highly dispersed CuO nanomaterial. Furthermore, the high-magnification FESEM images in Figures 2b and 2c highlight the distinct morphological features of the material, including a rough, sphere-like structure and a porous configuration, along with a broader size range.

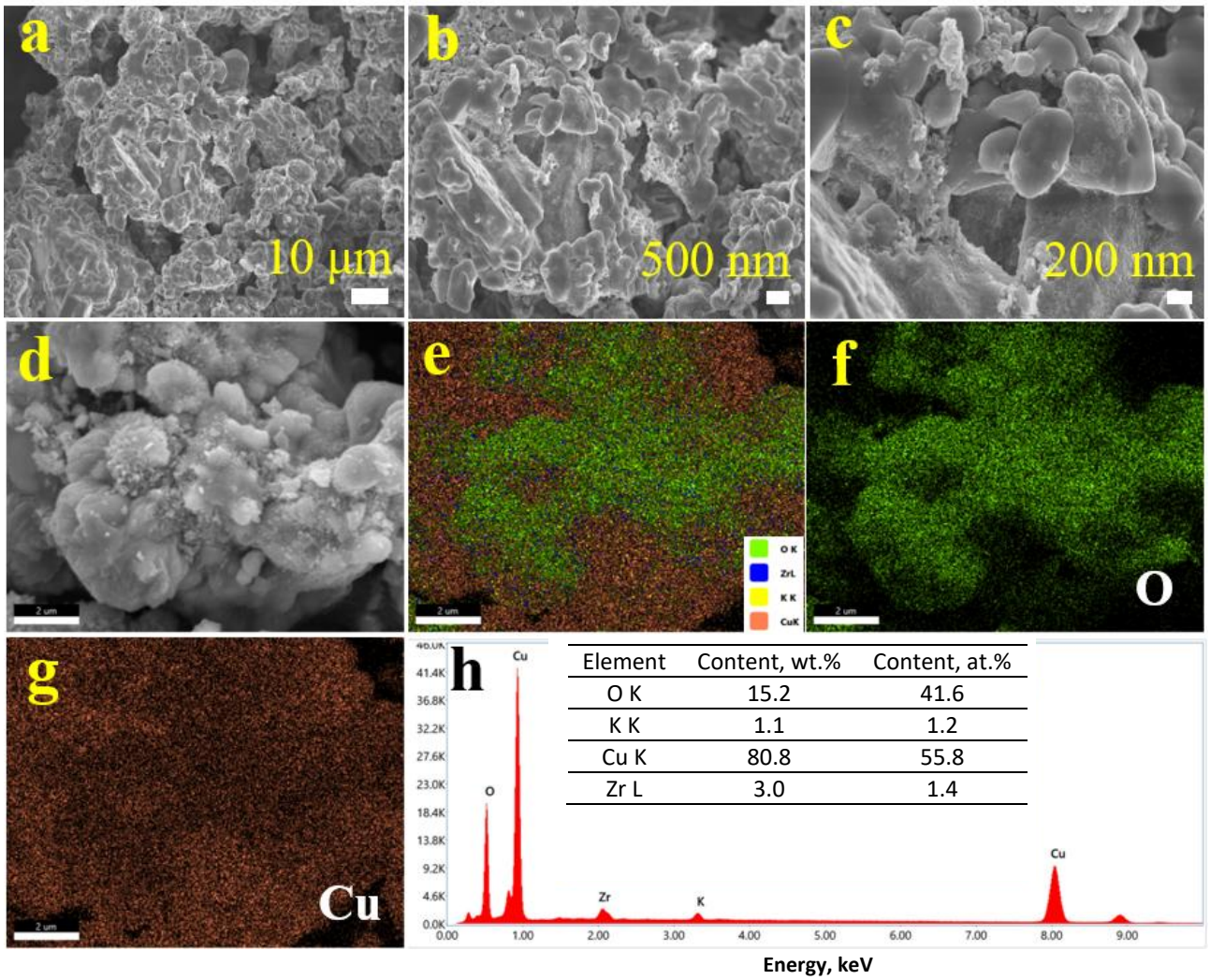

Element	Content, wt.%	Content, at.%
O K	15.2	41.6
K K	1.1	1.2
Cu K	80.8	55.8
Zr L	3.0	1.4

Figure 2. *(a-c) field emission scanning electron micrographs of CuO-NPs from lower to higher magnifications. (d-h) FESEM-EDS analysis: (d) live mapping, (e) elemental overlay image, (f) oxygen, (g) copper, (h) EDS spectrum and quantitative results. The white stripe indicates the scale bar*

The elemental mapping images of the CuO nanomaterial shown in Figures 2d-h confirm the presence of all the constituent elements (Cu and O) along with their measured ratio (inset of Figure 2h).

Similarly, the microstructural analysis and elemental composition of a specific region of the CuO@AC nanocomposite powder are presented in Figure 3. The nanostructure at low magnification is shown in Figure 3a, which depicts a surface covered with clusters of nanostructures exhibiting a rough, irregular, discrete, rubble-like morphology. The high-resolution FESEM images of the CuO@AC nanocomposite in Figures 3b and 3c are characterized by an irregular, blocky, or clumpy morphology resembling a mound of rubble. These structures are composed of numerous nanochunks and rugged, uneven surfaces arranged in a layered, cross-linked fashion radiating from the central core. The FESEM-EDS elemental mapping analysis of CuO@AC, as shown in Figure 3d-h, verifies the existence of each component element, including copper (Cu), oxygen (O), and carbon (C) as the major constituents of the prepared sample. The sharp peaks of EDX indicated in Figure 3i of the synthesized CuO@AC nanocomposite verify the existence of each component element in addition to their calculated composition, whereas a small amount of zirconium (Zr) in the sample was observed due to the impurities of metal used or contamination due to environmental effects in the prepared sample. The presence of a carbon peak in the prepared sample confirms the incorporation of carbon into the copper oxide nanoparticles during incineration and pyrolysis. Overall, the material's surface features indicate successful nanoarchitectonics of rubble morphology, with a homogeneous distribution of specific elements across the sample surface. Thus, the morphological characterization revealed increased porosity, interconnected nanorubbles, and a broad size distribution, indicating the potential of the biomass-derived activated carbon (BAC)- entwined copper oxide nanocomposite (CuO@AC) for electrocatalytic energy conversion processes such as HER, OER, and water splitting [6,30].

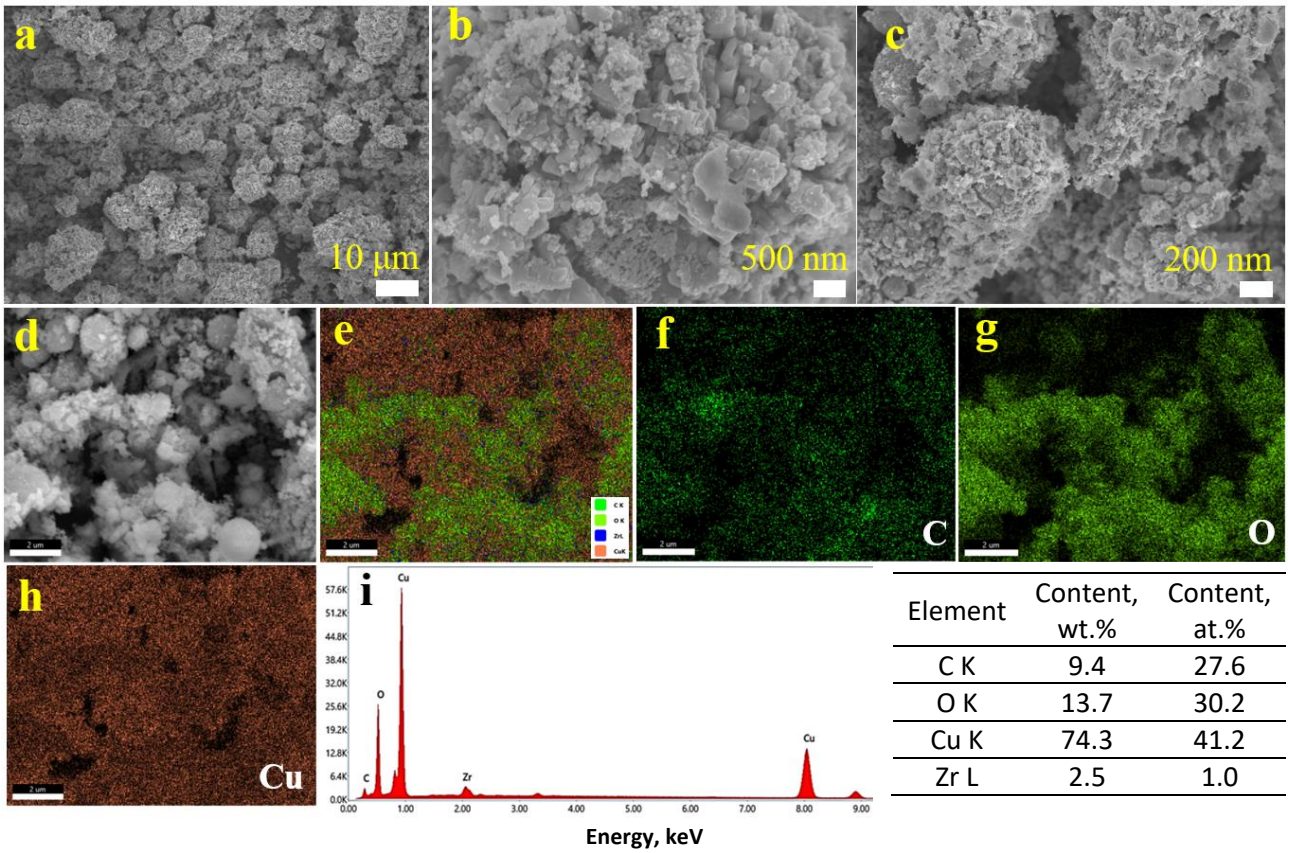

Element	Content, wt.%	Content, at.%
C K	9.4	27.6
O K	13.7	30.2
Cu K	74.3	41.2
Zr L	2.5	1.0

Figure 3. *(a-c) Field emission scanning electron micrographs of CuO@AC composite from lower to higher magnifications. (d-i) FESEM-EDS analysis: (d) live mapping, (e) elemental overlay image, (f) carbon, (g) oxygen, (h) copper, (i) EDS spectrum, and quantitative results. The white stripe indicates the scale bar*

Crystallographic study

XRD analysis of the samples was conducted to characterize the crystallographic properties of the resulting nanomaterials, serving as a non-destructive analytical method for identifying phases and unit-cell dimensions. Figure 4a shows the XRD patterns of the synthesized CuO and CuO@AC nanomaterials intended for electrochemical applications. The main diffraction peaks appeared at 2θ values of 32.4, 35.4, 38.7, 46.2, 48.7, 53.4, 58.3, 61.5, 65.7, 66.2, 67.9 and 72.4°, corresponding to Miller indices of (-110), (002), (111), (200), (-112), (202), (-113), (022), (-311), (113), (-220) and (311). The diffraction pattern also displayed two reflections at 2θ = 35.4° (002) and 2θ = 38.4° (111), indicating the formation of the monoclinic crystal phase of CuO. The lattice parameters are a = 0.46853 nm, b = 0.34257 nm and c = 0.51303 nm; these values align well with the standard JCPDS No. 00-041-0254 [17,35,41]. Lattice parameters are determined from XRD data by analysing the diffraction angles using Bragg's law and the Miller indices of the crystal planes. The measured interplanar spacings (d) are related to the unit-cell dimensions, thereby allowing calculation of the lattice constants [42]. Additionally, the crystal structure and phase composition of the copper oxide-entwined activated carbon (CuO@AC) nanocomposite were confirmed through XRD analysis, as evidenced by the orange coloration in Figure 4a. The prominent peaks at 32.46, 35.46, 38.74 and 48.91° closely match the crystal planes of a monoclinic phase of CuO (JCPDS No. 00-041-0254). Extra peaks observed at 2θ angles between 20 to 30° (corresponding to the 002 plane of graphitic carbon) and 40 to 50° (related to the 100 plane) strongly support the formation of a nanocomposite of CuO intertwined with activated carbon [34,36,41]. The multiple intense peaks in Figure 4a provide evidence for the successful fabrication of each expected crystalline phase, reflecting the overall composition and structural integrity of the nanomaterials.

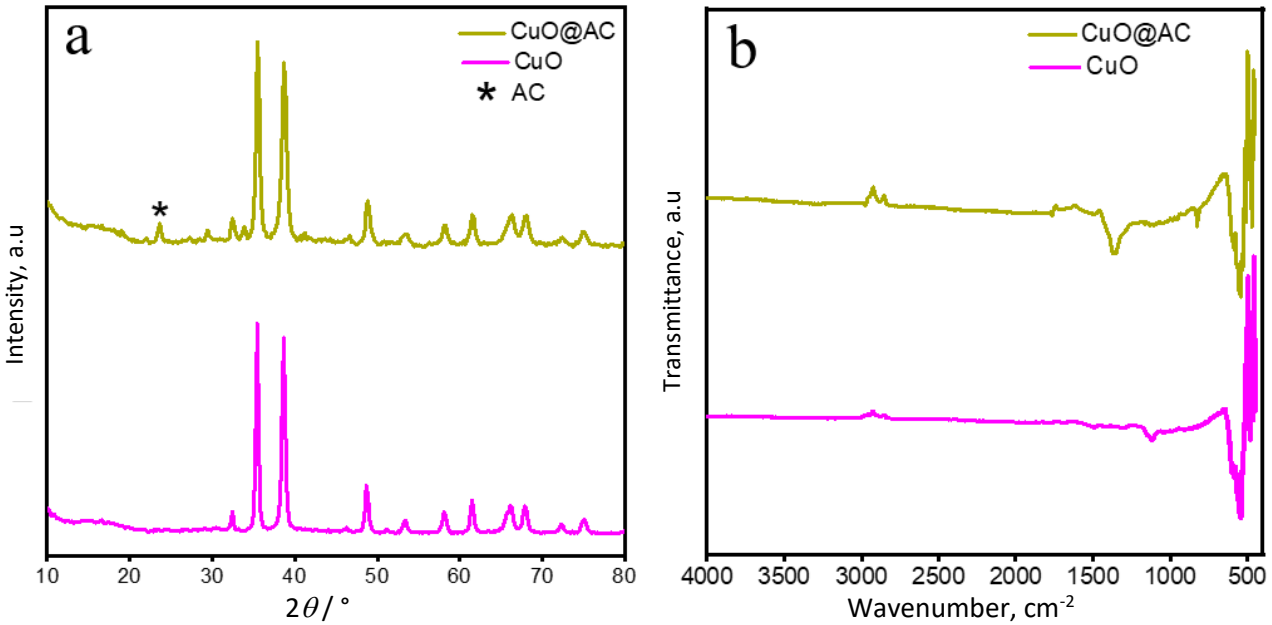

Figure 4. *(a) XRD patterns and (b) FTIR spectra of CuO and CuO@AC nanomaterials*

Spectroscopic study

The analytical configuration regarding the bonding and associated groups present in the nanomaterials (CuO and CuO@AC) was investigated using Fourier transform infrared (FTIR) spectroscopy at the wavelength range 4000 to 400 cm^{-1} (Figure 4b). The vibrational properties of CuO-NPs showed that the C-O stretching vibration is frequently linked to the absorption band at 1116.03 cm^{-1}, particularly of alcohols. The additional prominent bands around the fingerprint region, around 400

to 600 cm^{-1}, correspond to the Cu-O molecular fingerprint regions (Figure 4b). The broad vibrational properties of CuO@AC at 1000 to 1200 cm^{-1} are typically related to the C-O stretch, signifying the inclusion of biomass-derived carbon and formation of oxide during the activation process. Moreover, the most significant peaks at lower wavenumbers (400 to 600 cm^{-1}) can be attributed to Cu(II)-O bond vibrations (Figure 4b) [34,36,43].

Electrochemical HER study

To definitively assess the intrinsic electrocatalytic performance, we performed linear sweep voltammetry (LSV) on the electrode materials produced at a scan rate of 2 mV s^{-1} for the hydrogen evolution reaction (HER). The *IR*-corrected polarization curves are shown in Figure 5a. The *IR* correction aims to use the solution resistance (R_S) value for each electrode obtained using EIS to correct the electrode potential [30]. The overpotential was then calculated to reach the standard current density of 10 and 50 mA cm^{-2}. Figure 5b illustrates the overpotential (η_{HER}) for CuO-NPs estimated from the LSV polarization curve, which was 218 mV at a current density of 10 mA cm^{-2} and 315 mV at 50 mA cm^{-2}. In the meantime, to attain the current density of (10 and 50) mA cm^{-2}, the composite CuO@AC electrode needed an overpotential of 137 and 232 mV, respectively. The activated carbon (AC) exhibits no remarkable HER activity, with an overpotential of 380 mV at 10 mA cm^{-2}. Thus, the result shows that the CuO@AC has much more catalytic efficacy than the pristine CuO-NPs and AC catalysts, with good performance compared to that of the commercial Pt-C catalyst (Figure 5a-b). These excellent results are due to increased charge transfer, improved reaction kinetics, the formation of a more intense interface, and effective ion transport into sites and interfaces [44]. Moreover, the HER kinetics for the rate-determining step of the hydrogen evolution reaction were investigated using Tafel plots and Tafel slope values (Figure 5c), which were derived from the Tafel equation, $\eta = a + b \log J$ (b is Tafel slope, a is constant/Tafel intercept and J is current density) [16]. It was found that CuO@AC has the lowest Tafel slope value (94 mV dec^{-1}), compared with commercial Pt-C, CuO-NPs, and AC electrodes (137, 109, 224 mV dec^{-1}, respectively).

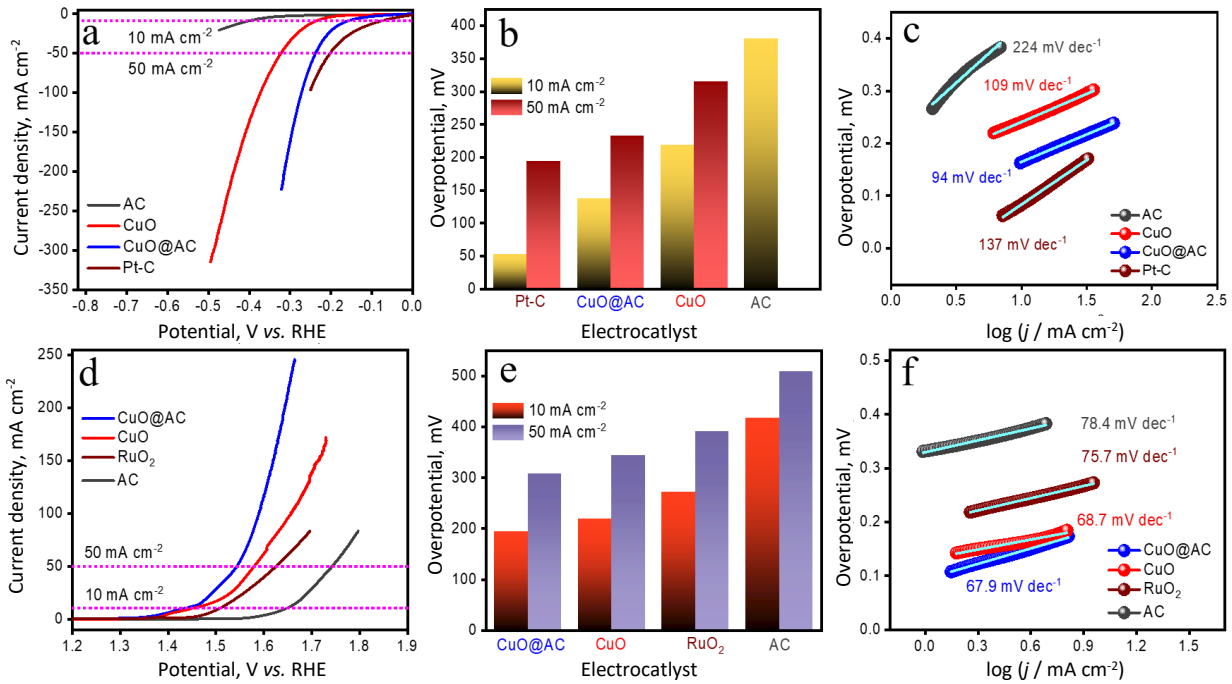

Figure 5. *Three-electrode HER/OER study at denoted electrocatalysts; (a) LSV polarization curves for HER after IR correction, (b) corresponding overpotentials, and (c) Tafel plots, (d) LSV polarization curves for OER after IR correction, (e) corresponding overpotentials, and (f) Tafel plots*

A larger Tafel slope indicates a slower reaction rate at the electrode-electrolyte interface; this leads to an increase in overpotential, since HER requires a high activation energy [45]. CuO@AC in an alkaline medium has a reduced Tafel slope value, indicating that the Volmer-Heyrovsky mechanism is in charge of processing HER. A specific electrochemical condition is suggested based on the intermediate Tafel slopes involving the Volmer mechanism (proton adsorption - dissociation of a water molecule on the catalyst surface, releasing adsorbed hydrogen and hydroxyl group) and the Heyrovsky mechanism (hydrogen recombination - release of H_2 molecule by combining solvated protons from electrolyte) [6,10].

Electrochemical OER study

We used LSV to examine the OER catalytic efficacy of the synthesized electrocatalyst at a sweep rate of 2 mV s^{-1}, and the *IR*-corrected polarization curves are shown in Figure 5d. The OER overpotential (η_{OER}) calculated from polarization curves at different current densities is plotted in Figure 5e [44]. The overpotential of individual electrocatalyst showed that CuO@AC, CuO-NPs, commercial RuO_2, and AC required an overpotential of 194, 219, 271 and 417 mV, respectively, to achieve a current density of 10 mA cm^{-2}. Similarly, an overpotential of 308 mV for CuO@AC, 343 mV for CuO, 391 mV for commercial RuO_2 and 509 mV for AC, respectively, was required to obtain a current density of 50 mA cm^{-2} (Figure 5e). The results demonstrated that CuO@AC is catalytically more efficient than alternative pristine electrocatalysts and the commercial RuO_2 because the supporting CuO nanoparticle on AC provides numerous accessible active sites, and well-dispersed nanoarchitecture [34,41]. Tafel slope analysis was also used to evaluate the OER kinetics of electrode materials (Figure 5f). The Tafel slopes for CuO@AC, AC, CuO-NPs, and RuO_2 were calculated to be (67.9, 78.4, 68.7 and 75.7 mV dec^{-1}), respectively. The Tafel slope of CuO@AC is the lowest among all synthesized materials, indicating superior performance in the OER pathway. This advantage arises from its efficient electrode kinetics, which enhance the interaction between the electrode and electrolyte, facilitated by a porous surface architecture [34,36].

Electrochemical impedance spectroscopy, cyclic voltammetry, double-layer capacitance and electrochemically active surface area analysis

Electrochemical impedance spectroscopy (EIS) measurements were carried out to elucidate the interfacial nature and capacitive behaviour of electrocatalysts in the active state, the charge-transfer process, and the electrochemical reaction kinetics. Figure 6a-b represents the resulting corresponding Nyquist plots (inset: equivalent circuit employed to model the impedance responses and the enlarged EIS plots) measured at the specific potential of the electrode at a fixed current density of 10 mA cm^{-2} during the HER and OER process, respectively [6]. Figure 6a-b depicts that the charge transfer resistance (R_{ct}) for AC is highest among the other counterparts. A lower R_{ct} value for the CuO@AC composite electrode than for the other control sample suggests a larger electrocatalytic surface area and improved charge transfer within the catalyst, resulting in significantly increased catalytic activity for HER and OER. Moreover, a lower solution resistance (R_s) for all electrocatalysts signifies minimized internal resistance, improved electrical conductivity, and a strong electronic interface between the catalyst and the electrode. Thus, the lower resistance at the electrode-electrolyte interface for CuO@AC indicates fast electron-transfer kinetics, a high charge-transfer rate, and a surface-capacitance feature, leading to enhanced overall reaction kinetics [10,13].

The double-layer capacitance (C_{dl}) was calculated based on the cyclic voltammetry approach at various scan speeds between 20 and 100 mV s^{-1}, based on the non-Faradaic potential window (1.12 to 1.24 V *vs.* RHE) as shown in Figure 6c-e. The capacitive current extracted from cathodic and anodic

sweeps in CV plots was used to assess the electrical double layer capacitance (C_{dl}) of the electrocatalysts [40]. The C_{dl} values calculated as linear fit to data points for CuO@AC, CuO, and AC were 2.49, 0.223 and 0.135 mF cm^{-2}, respectively (Figure 6f).

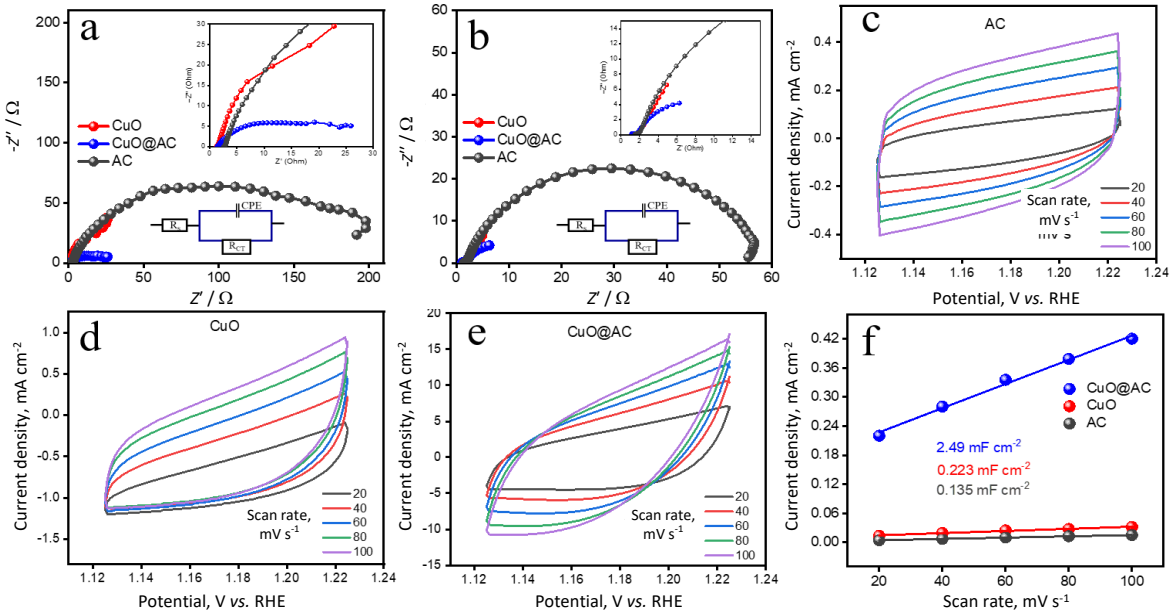

***Figure 6**: Nyquist plots of denoted electrocatalysts for (a) HER, (b) OER, (c) CVs at different scan rates of AC, (d) CuO, (e) CuO@AC, (f) current density (j) vs. scan rate and calculated C_{dl} values*

Higher C_{dl} values corresponded to higher ECSA, and as a result, the ECSA of the electrodes are in the order: CuO@AC > CuO-NPs > AC. The CuO@AC composite exhibits a higher ECSA than the corresponding pristine electrode, indicating greater catalytic effectiveness due to the increased number of catalytic sites [16]. Therefore, the catalytic efficiency of the CuO@AC, which is developed as an electrocatalyst, is expected to surpass that of the other materials.

Stability analysis and comparison with other works

The long-term stability of the CuO@AC catalyst was subsequently evaluated through accelerated durability testing, involving continuous cathodic (HER) and anodic (OER) current applications at 50 mA cm^{-2}. The chronopotentiometric (CP) analysis was conducted for approximately 12 hours in a three-electrode setup for individual HER and OER processes (Figure 7a).

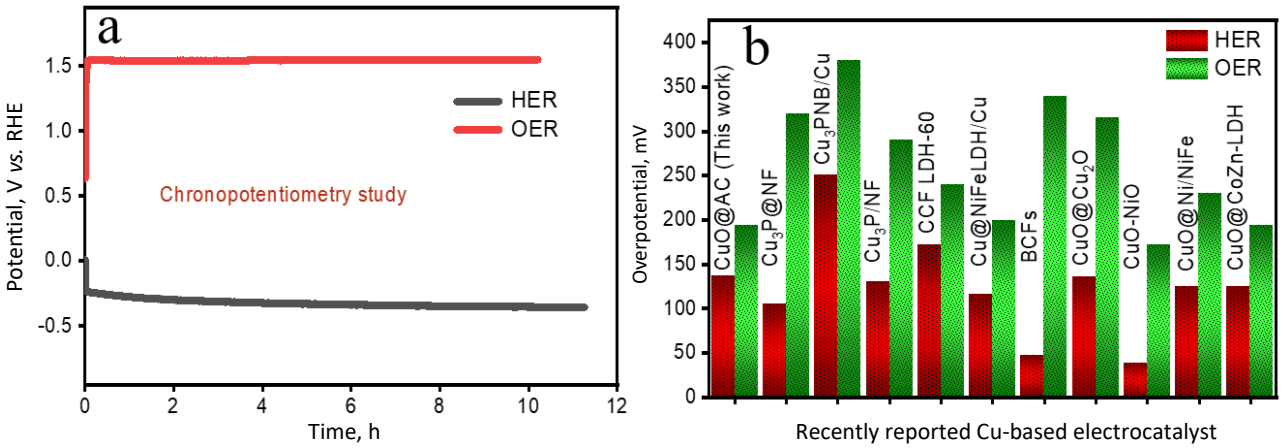

***Figure 7**: (a) chronopotentiometry stability test of CuO@AC for HER and OER; (b) comparison of recently reported Cu-based electrocatalysts for HER and OER*

The steady potential responses at a constant current of 50 mA cm^{-2} demonstrated the robustness of the electrocatalyst during prolonged operation for both HER and OER studies. Figure 7b compares the overpotential measured for CuO@AC with that of recently reported Cu-based electrocatalysts at 10 mA cm^{-2} in alkaline media. The results showed performance comparable to that of the reported electrodes, highlighting their superior efficacy [46-55].

Conclusions

In this work, we present a novel method for synthesizing biomass-derived activated carbon infused with CuO nanoparticles for efficient green hydrogen production *via* water splitting. The environmentally friendly synthesis of these copper oxide nanoparticles utilized *Allium sativum* extract and corncob biomass-derived activated carbon, ensuring a cost-effective and sustainable process with minimal hazardous chemicals. Structural and morphological characterization confirmed the properties of the well-synthesized nanomaterials. Moreover, the electrochemical performance of the CuO@AC composite was superior to that of CuO-NPs and AC for both HER and OER. CuO-NPs@AC exhibited lower overpotential (137 mV at 10 mA cm^{-2}) and Tafel slopes (94 mV dec^{-1}), indicating better catalytic activity than other contemporary pristine CuO-NPs and AC. Hence, the CuO@AC electrocatalyst exhibited low overpotential in symmetric water electrolysis and high efficiency, making it a promising, low-cost alternative for effective water electrolysis and green hydrogen production. This research could contribute significantly to sustainable energy technologies, promoting a net-zero emissions future for Nepal.

Acknowledgements: *The authors acknowledge sincere gratitude to the Department of Nano Convergence Engineering, JBNU (South Korea), NAST (Nepal) and Amrit Campus (TU, Nepal) for their research assistance, support and guidance. The authors appreciate UGC, Nepal, for financial support through the Faculty Research Grant.*

Funding: *There is currently no funding available for this research.*

Declaration of authors: *The authors declare that they have no conflicts of interest, financial or personal, that could influence the perception of this research.*

References

[1] D. Gielen, F. Boshell, D. Saygin, M. D. Bazilian, N. Wagner, R. Gorini, The role of renewable energy in the global energy transformation, *Energy Strategy Reviews* **24** (2019) 38-50. https://doi.org/10.1016/j.esr.2019.01.006

[2] R. Hanna, D. G. Victor, Marking the decarbonization revolutions, *Nature Energy* **6** (2021) 568-571. https://doi.org/10.1038/s41560-021-00854-1

[3] M. Singh, D. R. Paudel, H. Kim, T. H. Kim, J. Park, S. Lee, Interface engineering strategies for enhanced electrocatalytic hydrogen evolution reaction, *Energy Advances* **4** (2025) 716-742. https://doi.org/10.1039/d5ya00022j

[4] S. Gawusu, X. Zhang, A. Ahmed, S. A. Jamatutu, E. D. Miensah, A. A. Amadu, F. A. J. Osei, Renewable energy sources from the perspective of blockchain integration: From theory to application, *Sustainable Energy Technologies and Assessments* **52** (2022) 102108. https://doi.org/10.1016/j.seta.2022.102108

[5] M. Singh, D. C. Cha, T. I. Singh, A. Maibam, D. R. Paudel, D. H. Nam, T. H. Kim, S. Yoo, S. Lee, A critical review on amorphous-crystalline heterostructured electrocatalysts for efficient water splitting, *Materials Chemistry Frontiers* **7** (2023) 6254-6280. https://doi.org/10.1039/d3qm00940h

[6] D. R. Paudel, U. N. Pan, R. B. Ghising, P. P. Dhakal, V. A. Dinh, H. Wang, N. H. Kim, J. H. Lee, Interface modulation induced by the 1T Co-WS_2 shell nanosheet layer at the metallic $NiTe_2$/Ni core-nanoskeleton: Glib electrode-kinetics for HER, OER, and ORR, *Nano Energy* **102** (2022) 107712. https://doi.org/10.1016/j.nanoen.2022.107712

[7] M. A. Khan, H. Zhao, W. Zou, Z. Chen, W. Cao, J. Fang, J. Xu, L. Zhang, J. Zhang, *Recent Progresses in Electrocatalysts for Water Electrolysis,* Springer Singapore, 2018. https://doi.org/10.1007/s41918-018-0014-z
[8] M. Chatenet, B. G. Pollet, D. R. Dekel, F. Dionigi, J. Deseure, P. Millet, R. D. Braatz, M. Z. Bazant, M. Eikerling, I. Staffell, P. Balcombe, Y. Shao-Horn, H. Schäfer, Water electrolysis: from textbook knowledge to the latest scientific strategies and industrial developments, *Chemical Society Reviews* **51** (2022) 4583-4762. https://doi.org/10.1039/d0cs01079k
[9] X. Li, L. Zhao, J. Yu, X. Liu, X. Zhang, H. Liu, W. Zhou, Water Splitting: From Electrode to Green Energy System, *Nano-Micro Letters* **12** (2020) 131. https://doi.org/10.1007/s40820-020-00469-3
[10] D. R. Paudel, U. N. Pan, T. I. Singh, C. C. Gudal, N. H. Kim, J. H. Lee, Fe and P Doped 1T-Phase Enriched WS_2 3D-Dendritic Nanostructures for Efficient Overall Water Splitting, *Applied Catalysis B: Environmental* **286** (2021) 119897. https://doi.org/10.1016/j.apcatb.2021.119897
[11] J. Gautam, Y. Liu, J. Gu, Z. Ma, J. Zha, B. Dahal, L. N. Zhang, A. N. Chishti, L. Ni, G. Diao, Y. Wei, Fabrication of Polyoxometalate Anchored Zinc Cobalt Sulfide Nanowires as a Remarkable Bifunctional Electrocatalyst for Overall Water Splitting, *Advanced Functional Materials* **31** (2021) 2106147. https://doi.org/10.1002/adfm.202106147
[12] K. Chang, D. T. Tran, J. Wang, S. Prabhakaran, D. H. Kim, N. H. Kim, J. H. Lee, Atomic Heterointerface Engineering of Ni_2P-$NiSe_2$ Nanosheets Coupled ZnP-Based Arrays for High-Efficiency Solar-Assisted Water Splitting, *Advanced Functional Materials* **32** (2022) 2113224. https://doi.org/10.1002/adfm.202113224
[13] P. K. Joshi, S. Dahal, R. K. Rai, G. Bhandari, G. C. Kaphle, D. R. Paudel, Bifunctional Electrocatalysis of Copper-Doped Cerium Oxide Nanocage Networks Enabling HER and OER, *Electrocatalysis* **16** (2025) 844-855. https://doi.org/10.1007/s12678-025-00961-7
[14] J. Kibsgaard, I. Chorkendorff, Considerations for the scaling-up of water splitting catalysts, *Nature Energy* **4** (2019) 430-433. https://doi.org/10.1038/s41560-019-0407-1
[15] Z. W. She, J. Kibsgaard, C. F. Dickens, I. Chorkendorff, J. K. Nørskov, T. F. Jaramillo, Combining theory and experiment in electrocatalysis: Insights into materials design, *Science* **355** (2017). https://doi.org/10.1126/science.aad4998
[16] M. Singh, J. Park, H. Kim, G. Kim, D. Cha, D. R. Paudel, B. Kim, S. Lee, Heterointerface-Driven Electronic Modulation in MoO_2@N/Mo–ReS_2 Hybrid for Efficient Alkaline HER, OER, and Overall Water Splitting, *Small* **21** (2025) 2505906. https://doi.org/10.1002/smll.202505906
[17] S. Dahal, P. K . Joshi, N. S. Pandey, S. Gadal, D. R. Paudel, Bifunctional Hydrogen and Oxygen Electrocatalysis of Cerium Doped Copper Oxide Nanostructure, *Analytical and Bioanalytical Electrochemistry* **17** (2025) 311-326. https://doi.org/10.22034/abec.2025.723273
[18] P. Wang, J. An, Z. Ye, W. Cai, X. Zheng, Cu-Based Multicomponent Metallic Compound Materials as Electrocatalyst for Water Splitting, *Frontiers in Chemistry* **10** (2022) 913874. https://doi.org/10.3389/fchem.2022.913874
[19] J. A. Trindell, Z. Duan, G. Henkelman, R. M. Crooks, Well-Defined Nanoparticle Electrocatalysts for the Refinement of Theory, *Chemical Reviews* **120** (2020) 814-850. https://doi.org/10.1021/acs.chemrev.9b00246
[20] H. M. A. Amin, P. Königshoven, M. Hegemann, H. Baltruschat, Role of Lattice Oxygen in the Oxygen Evolution Reaction on Co_3O_4: Isotope Exchange Determined Using a Small-Volume Differential Electrochemical Mass Spectrometry Cell Design, *Analytical Chemistry* **91** (2019) 12653-12660. https://doi.org/10.1021/acs.analchem.9b01749
[21] H. M. A. Amin, M. Azimzadeh Sani, A. El Arrassi, S. Saddeler, S. Schulz, K. Tschulik, Probing the Intrinsic Oxygen Evolution Kinetics at Single $CoFe_2O_4$ Nano-Catalysts, *ChemCatChem* **17** (2025) e01234. https://doi.org/10.1002/cctc.202501234
[22] H. M. A. Amin, U. Apfel, Metal-Rich Chalcogenides as Sustainable Electrocatalysts for Oxygen Evolution and Reduction: State of the Art and Future Perspectives, *European Journal of Inorganic Chemistry* **2020** (2020) 2679-2690. https://doi.org/10.1002/ejic.202000406
[23] W. Yang, Z. Wang, W. Zhang, S. Guo, Electronic-Structure Tuning of Water-Splitting Nanocatalysts, *Trends in Chemistry* **1** (2019) 259-271. https://doi.org/10.1016/j.trechm.2019.03.006
[24] F. Song, L. Bai, A. Moysiadou, S. Lee, C. Hu, L. Liardet, X. Hu, Transition Metal Oxides as Electrocatalysts for the Oxygen Evolution Reaction in Alkaline Solutions: An Application-Inspired

Renaissance, *Journal of the American Chemical Society* **140** (2018) 7748-7759. https://doi.org/10.1021/jacs.8b04546

[25] H. A. Younus, Y. Zhang, M. Vandichel, N. Ahmad, K. Laasonen, F. Verpoort, C. Zhang, S. Zhang, Water Oxidation at Neutral pH using a Highly Active Copper-Based Electrocatalyst, *ChemSusChem* **13** (2020) 5088-5099. https://doi.org/10.1002/cssc.202001444

[26] J. Jeevanandam, S. F. Kiew, S. Boakye-Ansah, S. Y. Lau, A. Barhoum, M. K. Danquah, J. Rodrigues, Green approaches for the synthesis of metal and metal oxide nanoparticles using microbial and plant extracts, *Nanoscale* **14** (2022) 2534-2571. https://doi.org/10.1039/d1nr08144f

[27] H. M. A. Amin, H. Baltruschat, D. Wittmaier, K. A. Friedrich, A Highly Efficient Bifunctional Catalyst for Alkaline Air-Electrodes Based on a Ag and Co_3O_4 Hybrid: RRDE and Online DEMS Insights, *Electrochimica Acta* **151** (2015) 332-339. https://doi.org/10.1016/j.electacta.2014.11.017

[28] A. S. Sabir, E. Pervaiz, R. Khosa, U. Sohail, An inclusive review and perspective on Cu-based materials for electrochemical water splitting, *RSC Advances* **13** (2023) 4963-4993. https://doi.org/10.1039/d2ra07901a

[29] Z. Zhou, X. Li, Q. Li, Y. Zhao, H. Pang, Copper-based materials as highly active electrocatalysts for the oxygen evolution reaction, *Materials Today Chemistry* **11** (2019) 169-196. https://doi.org/10.1016/j.mtchem.2018.10.008

[30] D. R. Paudel, U. N. Pan, R. B. Ghising, M. R. Kandel, S. Prabhakaran, D. H. Kim, N. H. Kim, J. H. Lee, Multi-interfacial dendritic engineering facilitating congruous intrinsic activity of oxide-carbide/MOF nanostructured multimodal electrocatalyst for hydrogen and oxygen electrocatalysis, *Applied Catalysis B: Environmental* **331** (2023) 122711. https://doi.org/10.1016/j.apcatb.2023.122711

[31] Z. Chen, S. Yun, L. Wu, J. Zhang, X. Shi, W. Wei, Y. Liu, R. Zheng, N. Han, B. J. Ni, Waste-Derived Catalysts for Water Electrolysis: Circular Economy-Driven Sustainable Green Hydrogen Energy, Springer Nature Singapore, 2023. https://doi.org/10.1007/s40820-022-00974-7

[32] Z. Chen, W. Wei, H. Chen, B. J. Ni, Eco-designed electrocatalysts for water splitting: A path toward carbon neutrality, *International Journal of Hydrogen Energy* **48** (2023) 6288-6307. https://doi.org/10.1016/j.ijhydene.2022.03.046

[33] A. Muzammil, R. Haider, W. Wei, Y. Wan, M. Ishaq, M. Zahid, W. Yaseen, X. Yuan, Emerging transition metal and carbon nanomaterial hybrids as electrocatalysts for water splitting: a brief review, *Materials Horizons* **10** (2023) 2764-2799. https://doi.org/10.1039/d3mh00335c

[34] N. Prabu, T. Kesavan, G. Maduraiveeran, M. Sasidharan, Bio-derived nanoporous activated carbon sheets as electrocatalyst for enhanced electrochemical water splitting, International *Journal of Hydrogen Energy* **44** (2019) 19995-20006. https://doi.org/10.1016/j.ijhydene.2019.06.016

[35] M. Bin Mobarak, M. S. Hossain, F. Chowdhury, S. Ahmed, Synthesis and characterization of CuO nanoparticles utilizing waste fish scale and exploitation of XRD peak profile analysis for approximating the structural parameters, *Arabian Journal of Chemistry* **15** (2022) 104117. https://doi.org/10.1016/j.arabjc.2022.104117

[36] A. Q. Mugheri, A. Tahira, U. Aftab, M. I. Abro, A. L. Bhatti, S. Ali, M. A. Abbasi, Z. H. Ibupoto, A Low Charge Transfer Resistance CuO Composite for Efficient Oxygen Evolution Reaction in Alkaline Media, *Journal of Nanoscience and Nanotechnology* **21** (2021) 2613-2620. https://doi.org/10.1166/jnn.2021.19091

[37] M. Soltani, H. M. A. Amin, A. Cebe, S. Ayata, H. Baltruschat, Metal-Supported Perovskite as an Efficient Bifunctional Electrocatalyst for Oxygen Reduction and Evolution: Substrate Effect, *Journal of The Electrochemical Society* **168** (2021) 034504. https://doi.org/10.1149/1945-7111/abe8bd

[38] H. M. A. Amin, L. Zan, H. Baltruschat, Boosting the bifunctional catalytic activity of Co_3O_4 on silver and nickel substrates for the alkaline oxygen evolution and reduction reactions, *Surfaces and Interfaces* **54** (2024) 105218. https://doi.org/10.1016/j.surfin.2024.105218

[39] A. Rajput, A. Kundu, B. Chakraborty, Recent Progress on Copper-Based Electrode Materials for Overall Water-Splitting, *ChemElectroChem* **8** (2021) 1698-1722. https://doi.org/10.1002/celc.202100307

[40] D. R. Paudel, G. C. Kaphle, B. R. Poudel, M. KC, M. Singh, G. P. Ojha, Enhanced Hydrogen Evolution Reaction of a Zn^{+2}-Stabilized Tungstate Electrocatalyst, *Electrochem* **6** (2025) 3. https://doi.org/10.3390/electrochem6010003

[41] W. Zhang, R. Liu, Z. Fan, H. Wen, Y. Chen, R. Lin, Y. Zhu, X. Yang, Z. Chen, Synergistic copper nanoparticles and adjacent single atoms on biomass-derived N-doped carbon toward overall water splitting, *Inorganic Chemistry Frontiers* **10** (2022) 443-453. https://doi.org/10.1039/d2qi02285k
[42] G. Zampardi, J. Thöming, H. Naatz, H. M. A. Amin, S. Pokhrel, L. Mädler, R. G. Compton, Electrochemical Behavior of Single CuO Nanoparticles: Implications for the Assessment of their Environmental Fate, *Small* **14** (2018) 1801765. https://doi.org/10.1002/smll.201801765
[43] Y. Li, Y. Hu, W. You, G. Zhou, G. Peng, A facile method to fabricate AC/CuO for efficient removal of organic pollutants by adsorption and persulfate-based advanced oxidation processes, *Journal of Water Supply: Research and Technology - AQUA* **70** (2021) 20-29. https://doi.org/10.2166/aqua.2020.094
[44] D. R. Paudel, R. Kafle, N. Dhital, M. Singh, B. S. Salokhe, Nickel Nanoparticles Infused Iron Tungstate Nanocomposite for Clean Energy Carrier Hydrogen Generation via Water Splitting, *Advanced Materials Interfaces* **12** (2025) e00644. https://doi.org/10.1002/admi.202500644
[45] G. Bhandari, P. P. Dhakal, D. T. Tran, T. H. Nguyen, V. A. Dinh, N. H. Kim, J. H. Lee, Pt Single Atom-Doped Triphasic VP-Ni_3P-MoP Heterostructure: Unveiling a Breakthrough Electrocatalyst for Efficient Water Splitting, *Small* **20** (2024) 2405952. https://doi.org/10.1002/smll.202405952
[46] A. Han, H. Zhang, R. Yuan, H. Ji, P. Du, Crystalline Copper Phosphide Nanosheets as an Efficient Janus Catalyst for Overall Water Splitting, *ACS Applied Materials & Interfaces* **9** (2017) 2240-2248. https://doi.org/10.1021/acsami.6b10983
[47] S. Wei, K. Qi, Z. Jin, J. Cao, W. Zheng, H. Chen, X. Cui, One-Step Synthesis of a Self-Supported Copper Phosphide Nanobush for Overall Water Splitting, *ACS Omega* **1** (2016) 1367-1373. https://doi.org/10.1021/acsomega.6b00366
[48] J. Hao, W. Yang, Z. Huang, C. Zhang, Superhydrophilic and Superaerophobic Copper Phosphide Microsheets for Efficient Electrocatalytic Hydrogen and Oxygen Evolution, *Advanced Materials Interfaces* **3** (2016) 1600236. https://doi.org/10.1002/admi.201600236
[49] L. Yu, H. Zhou, J. Sun, F. Qin, D. Luo, L. Xie, F. Yu, J. Bao, Y. Li, Y. Yu, S. Chen, Z. Ren, Hierarchical Cu@CoFe layered double hydroxide core-shell nanoarchitectures as bifunctional electrocatalysts for efficient overall water splitting, *Nano Energy* **41** (2017) 327-336. https://doi.org/10.1016/j.nanoen.2017.09.045
[50] A. S. Sabir, E. Pervaiz, R. Khosa, U. Sohail, An inclusive review and perspective on Cu-based materials for electrochemical water splitting, *RSC Advances* **13** (2023) 4963-4993. https://doi.org/10.1039/d2ra07901a
[51] S. Hong, N. Song, J. Sun, G. Chen, H. Dong, C. Li, Nitrogen-doped biomass carbon fibers with surface encapsulated Co nanoparticles for electrocatalytic overall water-splitting, *Chemical Communications* **58** (2022) 1772-1775. https://doi.org/10.1039/D1CC06906C
[52] X.-X. Ma, L. Chen, Z. Zhang, J.-L. Tang, Electrochemical Performance Evaluation of CuO@Cu_2O Nanowires Array on Cu Foam as Bifunctional Electrocatalyst for Efficient Water Splitting, *Chinese Journal of Analytical Chemistry* **48** (2020) e20001-e20012. https://doi.org/10.1016/S1872-2040(19)61211-9
[53] Z. Guo, X. Wang, Y. Gao, Z. Liu, Co/Cu-modified NiO film grown on nickel foam as a highly active and stable electrocatalyst for overall water splitting, *Dalton Transactions* **49** (2020) 1776-1784. https://doi.org/10.1039/C9DT04771A
[54] Y. Liu, Z. Jin, X. Tian, X. Li, Q. Zhao, D. Xiao, Core-shell copper oxide @ nickel/nickel-iron hydroxides nanoarrays enabled efficient bifunctional electrode for overall water splitting, *Electrochimica Acta* **318** (2019) 695-702. https://doi.org/10.1016/j.electacta.2019.06.067
[55] L. Yin, X. Du, C. Di, M. Wang, K. Su, Z. Li, In-situ transformation obtained defect-rich porous hollow CuO@CoZn-LDH nanoarrays as self-supported electrode for highly efficient overall water splitting, *Chemical Engineering Journal* **414** (2021) 128809. https://doi.org/10.1016/j.cej.2021.128809